# He II Heat Transfer Through Superconducting Cables Electrical Insulation

B. Baudouy[a,]*, M. X. François[b], F.-P. Juster[a], C. Meuris[a]

[a]CEA-Saclay, DSM/DAPNIA/STCM, 91191 Gif-sur-Yvette Cedex, France
[b]CNRS/LIMSI, Bât. 502 ter, Campus Universitaire, 91405 Orsay, France

## Abstract

For NbTi magnets cooled by superfluid helium (He II), the most severe heat barrier comes from the electrical insulation of the cables. Tests on electrical multi-layer insulations, made of Kapton®, dry fiber and epoxy resin impregnated fiberglass tapes, indicate that heat transfer is influenced by He II contained in the insulation. Electrical insulation can be considered as a composite material made of a solid matrix with a complicated helium channels network. For several insulations, this network is characterized by steady-state heat transfer experiment through an elementary insulation pattern. Measurements in Landau regime for low temperature difference ($10^{-5}$ to $10^{-3}$ K) and in Gorter-Mellink regime for higher temperature differences permit to determine an equivalent He II channel cross section ($10^{-6}$ $m^2$) with an equivalent channel thickness (25 µm). We use the assumptions that He II heat transfer through the channels network and conduction in the insulation are decoupled and that the channels length is determined from the insulation overlap. It is observed that He II heat transfer is competing with conduction in the insulation. Furthermore, the measurements reveal an anomaly of heat transfer in the vicinity of the ? temperature which is associated to the phenomenon of ?-point depression.

*Keywords*: Electrical insulation (A); He II (B); Heat transfer (C); Accelerator magnets (F)

## Nomenclature

| | |
|---|---|
| A | Cross section ($m^2$) |
| (A) | Equivalent channel cross section ($m^2$) |
| ($Ad^2/L$) | Geometrical group of the equivalent channel in Landau regime |
| ($A/L^{1/3}$) | Geometrical group of the equivalent channel in Gorter-Mellink regime |
| d | Channel diameter (m) |
| (d) | Equivalent channel diameter (m) |
| e | Thickness (m) |
| $f$(T) | He II Equivalent thermal conductivity ($W^3/m^5K$) |
| k(T) | Thermal conductivity (W/m K) |
| l | Vortex line spacing (m) |
| L | Channel length (m) |
| T | Temperature (K) |
| $T_1$, $T_2$ | Boundary temperatures due to Kapitza resistance (K) |
| Q | Heat flux (W) |
| q | Heat flux density ($W/m^2$) |
| s | Entropy (J/KgK) |

*Greek Letters*

* Corresponding Author. Tel. : +33 (0)169084207 ; fax : +33 (0)169086929 ; email : baudouy@dapnia.cea.fr

| | |
|---|---|
| a | Kapitza coefficient ($W/m^2K^4$) |
| μ | Viscosity (Pa s) |
| ? | Coherence length (m) |
| ? | Density ($Kg/m^3$) |

*Subscripts*

| | |
|---|---|
| b | Cryostat bath |
| c | critical |
| cond | Conduction |
| GM | Gorter-Mellink |
| i | inner bath |
| L | Landau regime |
| m | mixed regime |
| n | Normal component of He II |
| s | Superfluid component of He II |
| t | total |
| ? | Related to the lambda transition |
| 8 | bulk property |

## 1 Introduction

Heat transfer studies in superconducting windings are of major importance for stability studies in accelerator magnets. For NbTi magnets cooled by superfluid helium, such as LHC dipoles, the thermal resistance created by the electrical insulation of the cables forms the main thermal resistance to He II cooling [1-2]. This is especially a problem in these magnets that are subjected to permanent thermal loads such as beam losses. Even if insulations are permeable to He II, current cooling of cables is insufficient to reach the specifications required by LHC designers [1]. For a better understanding and to define an appropriate insulation, thermal behavior of the insulation is approached through an experimental model [3-4]. The study, rather than considering a experiment on the entire heat transfer in a dipole, focuses on one-dimensional transverse heat transfer through an elementary insulation pattern, where conduction and He II heat transfer have to be considered.. Several insulations are tested in order to quantify their thermal performance to He II cooling.

## 2 Description of the electrical insulation sample

A typical insulation of a superconducting accelerator magnet is composed of a first layer, a tape wrapped around the cable providing the electrical insulation, and a second layer which has different functions such as protecting mechanically the first layer, creating helium channels and gluing to the adjacent conductor to keep the coil in shape for manipulation. Currently one or two wraps of Kapton® tapes, adhesive or not, with an overlap of 50 % are used for the first layer. For the second layer, adhesive Kapton®, epoxy resin impregnated (prepreg) fiberglass or reinforced Kevlar® fiberglass tapes wrapped with or without spacing are employed. For this experiment, 80 mm-diameter samples are constructed as plane slab and represent an elementary insulation pattern. Two insulation families are distinguished, the one with spacing of the second layer (Fig. 1-a) and the one without spacing but a dry fiber tape instead (Fig. 1-b). We present nine different insulations in Table 1. Insulations B6 and B16 can be seen as references. B6 corresponds to HERA dipole insulation. It is made of Kapton® HN tape overlapped by prepreg fiberglass wrapped with 2-mm spacing. B16 is an insulation tried for

SSC dipoles made of adhesive Kapton® as first layer and two wraps of adhesive Kapton® on both side of the tape as second layer. The adhesive is also a polyimide material which does not spread during curing. To investigate the influence of the material and spacing of the second layer, insulations B15, B18, B21 and B21' have been studied. The motivation to study B22, B22' and B25 was to investigate the influence of the first layer composition such as the material and the thickness. We present in Table 1 the samples thermal resistance and conductivity evaluated at 2 K, in conduction regime, taking into account the insulation components. To estimate their temperature dependency, these evaluations are made at 2 K and 4 K.

## 3 Experimental set-up and protocol

The experimental apparatus is composed of a stainless steel cylindrical support oriented vertically in the cryostat. A description of the experimental set-up is summarized in Fig. 2. Two 100-mm in diameter insulation samples are fixed over 20 mm of their diameter by 3M® DP190 epoxy resin and clamped by two stainless steel flanges, one on each side, to the cylindrical support to prevent helium leak. In that way it creates an isothermal inner bath where a heater and a temperature sensor are located. A capillary tube of 0.4-m length, carrying instrumentation wires is wrapped around the cylindrical support and insulated by Stycast® epoxy resin. Heat leak through the capillary tube is negligible compared to the heat dissipated for the range of power investigated [2]. Tests have been performed in pressurized He II and in saturated He II. The temperature difference accuracies are about 1 mK and 10 µK respectively, using an a.c. bridge resistance equipped with a lock-in null detector. Thermometers used are Allen Bradley resistors calibrated in situ.

After attaining stationary temperature for both baths, temperature measurement is made. The cryostat bath temperature $T_b$, is regulated and held constant ( 2 mK)for the whole test over the range of power dissipation. The measured temperature difference characterizes the overall thermal resistance between the inner and the outer bath that includes the Kapitza resistance on the insulation boundary, the thermal resistance of the insulation itself and the one of the helium channels through the insulation.

## 4 Heat transfer characteristic curves

Figure 3 presents results obtained with two different experiments in pressurized and saturated helium for sample B22 at a bath temperature of 1.9 K. The bath temperature of the two experiments is the same within 1 mK over the heat flux range. With heat flux increasing, the curve exhibits successively the Landau and the Gorter-Mellink regime separated by a transition regime. For comparison, it is displayed a "conduction curve" which takes into account conduction and Kapitza resistance. The Kapitza resistance has been measured on Kapton® HN at STCM [5]. The Landau regime ends when the heat flux reaches a critical heat flux $Q_c$ where superfluid turbulence appears. In the Landau regime, the normal fluid flow can be either laminar with a linear relation between ? T and Q ($\vec{q} = (?sd)^2 T\vec{\nabla}T/12\mu$), or turbulent, in a classical way, with a non linear relation $\Delta T=f(Q^{1.75})$ deduced from the Blasius law [6]. In our experiments, the Landau regime is found to be linear for all the samples. The transition between the two regimes delimited by $Q_c$, the end of the Landau regime, and $Q_{GM}$, the onset of Gorter-Mellink, is not so well marked because it corresponds to the nucleation and development of vortices in the superfluid component. As the channels have different diameters distributed between a minimum and a maximum value, the critical velocities for the vortices nucleation are also distributed between a minimum and a maximum value. Therefore, one considers Landau regime ends at $Q_c$ when vortices appear in the largest channels and Gorter-Mellink regime starts at $Q_{GM}$ ($q^2\vec{q} = f(T)\vec{\nabla}T$) where superfluid turbulence is fully developed in the smallest channels. The effect of channel diameter will be also sensitive close to the ?-point. Note that the equivalent thermal conductivity is, as expected, higher in the Landau regime than in Gorter-Mellink regime. Moreover, even if conduction in the insulation is present for the all heat flux range, it is negligible compared to He II heat transfer for this sample and most of the others.

Otherwise we face another regime particular to our system, that we named the "mixed regime". It is reached for the heat flux $Q_m$ where conduction is no longer negligible compared to He II heat transfer. As the heat flux increases in the mixed regime, the slope of the curve decreases because the conduction in the insulation is not negligible anymore. This is in agreement with the fact that the He II equivalent thermal conductivity decreases rapidly with temperature approaching $T_?$ that is for large temperature difference. Note that mixed regime is better than pure He II heat transfer which is given by the dashed line in Fig. 3. As the temperature is reaching $T_?$, He II heat transfer decreases compared to conduction. The mixed regime ends for a heat flux Q* when the temperature of the inner bath, $T_i$, reaches $T_?$. One can note that the experimental curve does not meet the conduction curve at Q* because only helium in the channels close to the inner bath side undergoes the phase transition, i.e. at $T_i=T_?$, there is still He II participating to heat transfer. Data cannot be analyzed for $T_i>T_?$ because the inner bath is no longer isothermal, that is the principle of the experimental set-up.

As presented above, critical heat fluxes $Q_c$ and $Q_{GM}$ depend on the geometrical dimensions of the helium network and thermodynamic properties of helium whereas Q* and $Q_m$ depend also on conduction characteristics of the insulation. The evaluation of $Q_m$ deserves a definition regarding the thermal model. The principal aim of this description is to emphasize on the fact that the overall thermal characteristic of the insulation depends on channel dimensions in He II dominant regime as well as on the sample thermal properties in the mixed regime.

## 5 Model and analysis method of experimental results

The analysis of the results is based on the assumption that He II heat transfer in the channels and conduction in the insulation are independent as simplified in Fig. 4. This assumption is verified with a 2D numerical computation. The calculation considers a helium channel, as it is created by the overlap of the first layer, with a 11-mm length delimited by Kapton® (The tape has a 11-mm width and is overlapped with a 30° angle) [2]. The insulation thickness (Kapton®) is 25 µm with a 50% overlap. The thickness of the channel is varied from 1 µm to 20 µm. These values are in the order of magnitude of the ones determined from experimental results. The heat transfer mechanisms considered are Gorter-Mellink regime in helium and conduction in the insulation. Kapitza resistance is also modeled on the contact surface between the helium and insulation.

For a bath temperature of 1.9 K and an overall temperature difference of 50 mK across the system, the heat paths are parallel for channel thickness comprised between 1 to 20 µm. For bath temperatures of 1.7 K and 1.8 K, heat flux coming out is less than a percent higher than the heat flux entering the channel whereas for bath temperature of 2.0 K and 2.1 K, the heat flux coming out is lower. It means that a part of the heat entering the channel is not carried until the end but goes through the insulation. These calculations indicate that the coupling is negligible between the two heat transfer mechanisms.

For a higher temperature difference of 0.25 K, at 1.9 K, 14 % of the heat flux carried by the channel at the entrance goes through the insulation. Calculations performed for higher temperature difference with bath temperatures give approximately equivalent results. When $f(T)$ is increasing, for bath temperature inferior to 1.95 K, the heat flux in the channel is higher at the exit than at the entrance and with $f(T)$ decreasing, the heat flux is lower at the exit.

We consider the assumption of parallel heat transfer paths valid for channel thickness considered and different bath temperatures, nevertheless we expect some discrepancy with the experimental data for large temperature difference. The total heat flux is then given by:

$$Q = Q_{He\,II} + Q_{cond} = Q_{He\,II} + \frac{A_{cond}}{e_{cond}} \int_{T_1}^{T_2} k(T)dT, \qquad (1)$$

where $Q_{He\ II}$ represents the heat flux in the helium channel network whereas $Q_{cond}$ represents conduction in the insulation. $A_{cond,}$ $e_{cond}$ and k(T) are respectively the thickness, the cross section and the conductivity of the insulation. Considering that the cross section of the channels is negligible compared to the insulation's one, $A_{cond}$ is equal to the sample's cross section $A_{cond}=A_t$. $T_1$ and $T_2$ are the unknown boundary temperatures of the insulation given by Kapitza boundary conditions. $T_b$ and $T_i$ are respectively the temperature of the cryostat bath and the inner bath. In the small $\Delta T$ assumption of the phonon radiation limit, heat flux transferred at this boundary is:

$$Q_{cond} = 4aA_t T_b^3 (T_1 - T_b) = 4aA_t T_i^3 (T_i - T_2). \quad (2)$$

a has been measured on Kapton® HN at STCM [5]. The insulation overlap creates a network of N distinct channels of different thickness submitted to the same temperature difference, that is to say that they are considered thermally in parallel.

We propose to regard this network as a single channel, equivalent in terms of heat transport property, with the appropriate geometrical characteristic, length L, thickness d, and cross section A**.** Heat flux in Landau regime is written for channels having rectangular cross section with large aspect ratio [7]:

$$Q_{He\ II} = \sum_{n=1}^{N} \frac{A_n d_n^2}{L_n} \int_{T_b}^{T_i} \frac{(?s)^2 T}{12\mu} dT = \left( \frac{Ad^2}{L} \right) \int_{T_b}^{T_i} \frac{(?s)^2 T}{12\mu} dT. \quad (3)$$

$A_n$, $d_n$ and $L_n$ represent respectively the cross section, the thickness and the length of a channel. s, μ and ? are respectively the entropy, viscosity and density of helium. Notation $(Ad^2/L)$ represents the geometrical group of the equivalent channel. In Gorter-Mellink regime, the heat flux is written with the geometrical group $(A/L^{1/3})$ for the equivalent channel as:

$$Q_{He\ II} = \sum_{n=1}^{N} \frac{A_n}{L_n^{1/3}} \left[ \int_{T_b}^{T_i} f(T) dT \right]^{1/3} = \left( \frac{A}{L^{1/3}} \right) \left[ \int_{T_b}^{T_i} f(T) dT \right]^{1/3}. \quad (4)$$

Analysis of the experimental results is realized for the Landau and Gorter-Mellink regimes. As mentioned above, the difficulty of analysis is to define the heat flux range for the corresponding regimes. The analysis is realized in a heat flux range where conduction is negligible compared to the total heat flux. In that range the total heat flux is identified to the one carried by the helium channels and data are fitted by the appropriate law given by (3) or (4). An example of analysis is presented in Fig. 3 where can be distinguished the Landau and Gorter-Mellink regions for which the groups $(Ad^2/L)$ and $(A/L^{1/3})$ are determined. These regimes are defined by the best fit of the data based on equations (3) and (4); consequently it defines also the critical heat flux $Q_c$ and $Q_m$ which are arbitrarily the value of Q when $Q_{cond}$ reaches 10% of Q. Table 2 gives the results of the determination of the two groups as a function of bath temperature for sample B22. The precision of the calculation includes the precision of both measurements and fit. $(Ad^2/L)$ is dropping with increasing temperature and is given with a precision comprised between 10 % and 20 %. $(A/L^{1/3})$ is given with a better accuracy (inferior to 7 %) because the number of data points is higher than in Landau regime. Its value is almost constant, which gives confidence in the analysis method, excepted for the higher value at 2.1 K. The temperature dependence is found for $(A/L^{1/3})$ for other samples. When conduction is no longer negligible, as for samples B16 and B25, whatever the heat range considered, the regime corresponds to a mixed regime. It is necessary then to take into account conduction to determine the geometrical groups of the channel network.

Figure 5 presents the comparison between model and measurement for sample B15 at $T_b$=1.902 K in the Gorter-Mellink and mixed regimes. This sample is taken as an example because conduction is not negligible

for the entire heat flux range. The part of conduction is 36 % at Q*. For low heat flux, the model predicts a lower heat flux because ($A/L^{1/3}$) is determined neglecting the conduction. In the mixed regime, the difference between the model and experiment does not exceed 10 % even at Q*. It confirms that the method of analysis (and consequently the model) reproduces with good accuracy the physical phenomenon (considering that insulation thermal properties are known with a precision of 20 % in average). Same observations can be made at different bath temperatures. For other samples, the difference between model and experimental data is not higher than 20 %.

## 6 Experimental results and analysis

Figure 6 presents the ensemble of the results at the bath temperature of 1.9 K where temperature difference is plotted as a function of the normalized heat flux to $A_t$ ($q=Q/A_t$). This figure displays also an average conduction curve constructed from average sample properties. The gray surfaces represents the different regimes that have been obtained experimentally after analyzing the samples. They have been constructed from the evolution of the different normalized heat flux $q_c$, $q_{GM}$, $q_m$ and q*. The more permeable to He II the sample is, the further the heat transfer curve is far from the curve representing a pure conduction regime whereas the curves associated to non permeable sample are close to this limit. The curve slope of permeable samples is higher than the conduction curve even close to the ? transition, showing the He II heat transfer effect. The curve slope and q* increase as the samples is more permeable to He II. Table 3 presents the results of the determination of the geometrical groups at 1.8 K. Only three samples have been tested at low temperature differences (B22, B22' and B25). The higher ($Ad^2/L$) and ($A/L^{1/3}$) are, the more permeable to He II the samples become.

### *6.1 Non permeable samples*

For samples B16 and B25, the determination of ($A/L^{1/3}$) was not possible because the dominant heat transfer is conduction over the entire range of heat flux. Heat transfer curves for B16 and B25 are entirely located in the upper domain of the mixed regime and exhibit the same linear behavior especially at low heat flux. B16 is composed of a second layer made of adhesive Kapton® on both sides wrapped with a 50 % overlap and a first layer made of adhesive Kapton® on the external side. B25 has a 2-mm spaced adhesive Kapton® second layer and a first layer made of two wrappings. One can conclude that when the second layer is adhesive on both side or when the first layer is doubled, the permeability to He II is drastically reduced.

### *6.2 Influence of the first layer*

Few experiments on the influence of the first layer have been performed because the second layer was first considered as the driving parameter and because technically the first layer was supposed to remain unchanged. B22' and B25 differ by the first layer which a double 50 % overlapped Kapton® wrap for B25 whereas for B22' it is realized with one layer. B22 exhibit a permeable behavior and B25 heat transfer curve exhibits a "conductive" behavior (Fig. 6). $(Ad^2/L)/A_t$ is 6 time higher for B22' than for B25 (Table 3). A double Kapton® wrap reduces the number of open channels and creates a non-permeable insulation.

### *6.3 Influence of the second layer*

The spacing of the second layer is a parameter that has been studied with samples B22 and B22'. B22 has a 4-mm spacing, which should increase the number of open channels (or the section of these channels), whereas B22' has a 2-mm spacing. This picture seems to be realistic since the B22 heat transfer curve is lower than B22''s one. $(A/L^{1/3})/A_t$ ratio is around 5.9 between B22 and B22'. Difference between heat transfer curves

and $(A/L^{1/3})/A_t$ groups between B22 and B22' shows that increasing spacing for a Kapton-Kapton® type insulation improves heat transfer.

The material used for the second layer has been also investigated. The comparison of B6 and B15 shows that B15 is more permeable to He II than B6. B15 group $(A/L^{1/3})/A_t$ is roughly 4 times higher than B6's one. The epoxy resin contained in the fiberglass tape of B6 flows during curing and fills up the available channels. To enhance the transverse heat transfer, it is preferable to use a second layer with polyimide glue which is used as a countermeasure against spreading.

B18 does not exhibit spacing on the second layer (Fig. 1-(b)) but a prepreg fiberglass and a dry fiber tape wrapped side by side. One can expect that the dry fiber tape of 10.5 mm would increase permeability but B6 for small ? T is more effective than insulation B18 whereas for high ? T, their thermal behavior is identical. The combination of prepreg fiberglass and dry fiber tape does not improve the transverse heat transfer.

B21' has been constructed from insulation B21 in eliminating the dry fibers tape. It is interesting to note that even if the fiber tape of B21 is epoxy free, temperature differences for B21 are in average an order of magnitude higher than for B21' for the same heat flux. Even if the thermal behavior of these two insulation is dominated by He II heat transfer, one can note that $(A/L^{1/3})/A_t$ of B21' is 2.16 times higher than B21's one, suggesting that the dry fiber cloth tape reduces the number of emerging channels.

Insulations B18 and B21 are type (b) insulation (Fig. 1). B21 has an insulation composed of adhesive Kapton® and dry fiber tapes whereas for B18 the Kapton® tape is substituted by prepreg fiberglass tape. B21 $(A/L^{1/3})/A_t$ group is 8 times higher than B18's one, confirming that epoxy resin flows and fills up the channels. One can add by looking at the sample itself that it seems that the permeability comes also from the fact that the cloth and the Kapton® tape do not glue to each other, on the contrary of sample B18 where adhesion is made by the epoxy resin.

## 7 Dimension of the channels

The model applied to the channels network allows to determine the geometrical groups $(Ad^2/L)$ and $(A/L^{1/3})$. We present simple assumptions that permit to determine the equivalent thickness (d) and cross section (A). The parenthesis notation is kept to recall that they are equivalent parameters. We consider that the channels have the same length, L, equal to the average length of the width of the overlap created of the first layer. Note that for B22 and B22', the Kapton® tape has a 11-mm width and is overlapped with a 30° angle then the average length is equal to 11 mm. Then, from the group $(A/L^{1/3})$, we can deduce an equivalent cross section,

$$(A) = L^{1/3}\left(\frac{A}{L^{1/3}}\right) \tag{5}$$

(d) can be deduced from the coefficient $(Ad^2/L)$ and (5),

$$(d) = \sqrt{\frac{L}{(A)}\left(\frac{Ad^2}{L}\right)} = L^{1/3}\sqrt{\left(\frac{Ad^2}{L}\right)\Big/\left(\frac{A}{L^{1/3}}\right)} \tag{6}$$

It may be noticed that this assumption implies that L and (d) are supposed to be constant in Landau and Gorter-Mellink regimes. We present (d) and (A) in Table 4 for sample B22 and B22' as a function of the bath temperature. We retain only average values between 1.7 K and 2.0 K. B22 has an equivalent thickness of 27.5 µm and cross section of 6.9 $10^{-6}$ $m^2$ and B22' has an equivalent thickness of 18.8 µm and a cross section of 2.6 $10^{-6}$ $m^2$.

From these average values, it is important to check if the normal fluid flow in the Landau regime is laminar to confirm that the law we used to determine the equivalent coefficient fits the physical phenomenon. Using the normal fluid velocity corresponding to the critical heat flux, a Reynolds number, based on the normal velocity [6], can be calculated based on the geometrical equivalent parameters (d) and (A), and

$$\mathrm{Re} = \frac{?(d)v_n}{\mu} = \frac{(d)}{(A)}\frac{Q_c}{\mu sT}. \qquad (7)$$

This maximum Reynolds number of the Landau regime is around 100 [2]. These values, always inferior to the admitted critical Reynolds number value of 1200, confirm that the fluid dynamics regime is always laminar [6]. It is also important to verify that the average confinement found in the insulation do not modify the characteristics of superfluid turbulence. The dominant criteria preventing superfluid turbulence to be fully developed in our system is related to the vortex lines spacing. The vortex line spacing $l$ has to be much smaller than the smallest dimension of the media. This criteria is given by $l < (d)$ and Vinen gives a good approximation of the temperature evolution of $l\,|\vec{v}_n - \vec{v}_s|$ [8]. An equivalent critical velocity of the superfluid component can be build using the equation $?_s|\vec{v}_n| + ?_n|\vec{v}_s| = 0$ and experimental results can be compared with Vinen's expression. One find out that $l$ is at least an order of magnitude lower than the equivalent thickness of samples B22 and B22' over the entire range of heat flux [2]. It means that the turbulence is fully developed and that the use of the Gorter-Mellink law is justified for our system.

## 8 Measurement in the vicinity of the ?-point

In the Landau regime for sample B22', temperature dependence of the curves in Fig. 7 follows the dependence of $(?s)^2T/\mu$ until a bath temperature of 2.0 K whereas for higher temperatures, the dependence reverses. For example, at 2.109 K, the curve is located between the 1.9 K et 2.0 K curves. Other measurements show that the closer the bath temperature is to $T_?$ the higher the curve is revealing that a heat transfer degradation arises in the vicinity of the ?-point [2]. As a result of this degradation, the group $(Ad^2/L)$ decreases drastically at 2.05 K as it is shown in Fig. 8. Nevertheless, $(Ad^2/L)$ undergoes a smaller decrease starting from 1.7 K. One can remark that there is an order of magnitude difference of $(Ad^2/L)$ between 1.7 K and 2.15 K. A similar evolution is found for sample B22 between 1.7 and 2.1 K (Fig. 8). The temperature dependence of $(Ad^2/L)$ could be seen as a decrease of the channels cross section participating to He II heat transfer as the bath temperature is reaching $T_?$.

This anomaly suggests that this effect is due to the disappearance of superfluid properties while approaching $T_?$. In the theory of superfluidity, the superfluid density $?_s$ is null at the wall and increases to its bulk value beyond a characteristic length: the so-called coherence length. Ginzburg and Pitaevskii wave function theory (? -theory) demonstrates that the coherence length tends to infinite as $?=?_8(T_?-T)^{-2/3}$ when the temperature is approaching $T_?$ [9]. In confined environment when the temperature tends to $T_?$, the coherence length can be in the order of magnitude, or more, of the medium dimension and one can expect some superfluidity "defects". In this situation, the confined liquid has a superfluid density inferior to the liquid bulk density, which means that the $T_?$ is inferior to the bulk one. This phenomenon, known as the ?-point depression, has been theoretically predicted by the "? -theory" and measured experimentally by different groups [10-11].

To understand the effect of the depression of the ?-point on heat transfer in our system, we need to consider that the channel network is composed with different channel sizes. At temperature close to 1.7 K, the coherence length is small and the entire network of channels is participating to heat transfer. This is the reason why the coefficient $(Ad^2/L)$ is almost constant with the bath temperature. One can note that there is a slight decrease which suggests that the effect might be present at these temperatures in the smallest channel. With the bath temperature increasing, the coherence length is increasing and reaching the size of the smallest

channels or eventual restriction along the channels. At these location, helium undergoes a phase transition and He I appears in these channels. The He I volume acts as a “thermal and dynamical plug” for the concerned channels which are excluded from the He II channels network. It is equivalent to say that the cross section of the channels participating to He II heat transfer is lower than the one at lower bath temperature.

In Fig. 8, evolution of $(Ad^2/L)$ suggests that the curve goes to zero at a temperature lower than $T_?$ which is around 2.153 K. If this temperature is retained as $T'_?$, the evolution of $(Ad^2/L)$, between 2.08 K and 2.15 K, can be fitted by $2{,}4\ 10^{-13}(T'_?-T_b)^{0{,}49\ \ 0.04}$ (Fig. 9). On this figure, the value of $(Ad^2/L)$ at 2.148 K is aberrant to our point of view and we can note that the fit of $(Ad^2/L)$ evolution gives without this point $2{,}4\ 10^{-13}(T'_?-T_b)^{0{,}43\ \ 0.04}$. The theoretical evolution of the superfluid density is $?_s=?_{s8}(T_?-T_b)^{2/3}$ [9]. According to Eq. (3) the evolution of $(Ad^2/L)$ should be comparable to the square of the superfluid density evolution that is to say $(T_?-T_b)^{4/9}$. The good agreement of the measurements with theory suggests that the phenomenon encountered is the ?-point depression. Moreover, Ginzburg et Pitaevskii showed for a helium film that the depression of ?-point can be approximately related to the characteristic dimension of the medium d by $? T_?=2\ 10^{-14}/d^2$ [12]. It gives in our case a thickness of 1 µm which can be associated to the restriction size in our insulation, probably located at the overlap of the first layer. This dimension is in the order of magnitude of the vortex line spacing. In this condition the superfluid turbulent might not be fully developed and it can explain, for bath temperature higher than 2.0 K, the decrease of the group $(A/L^{1/3})$ when the bath temperature is increasing (Table 2).

## 9 Conclusion

Results show clearly that insulation creates a network of helium channels and that a simplified He II thermodynamic model allows to identify the contribution of that network on the total heat transfer. The proposed model predicts with an accuracy of 20 % that heat transfer through insulation is a parallel heat transfer between the conduction in the insulation itself and He II heat transfer in the network. In the Landau regime, when the temperature is approaching $T_?$, an anomaly in the heat transfer has been identified. We are proposing a explanation based on the phenomenon of the depression of the ?-point where the superfluid properties are altered. This effect occurs for dimensions in the order of magnitude of the micrometer which lets us assume that such restrictions of that dimension exist in the channels. They could be located at the first layer overlap.

The results and the method of analysis allow a detailed qualification of the insulation permeability to He II by determining geometrical groups. Under our assumptions, average channel thickness of the order of 25 µm and cross section of the order of $10^{-6}$ $m^2$ can be extracted. This qualification permits to bring out the principal characteristics to improve heat transfer through insulation. We can conclude that a second layer made of adhesive Kapton on both side or a double Kapton® wrap in the first layer reduces the permeability to He II. Dry fiber cloth tape or a combination of prepreg fiberglass and dry fiber tape in the second layer has the same effect. The ideal insulation should be composed of a non-adhesive Kapton® tape as a first layer and a second layer made of adhesive (on the external side only) Kapton® tape wrapped with spacing.

## Acknowledgments

The authors are grateful to A.- M. Puech and R. Gaubert for the sample preparation and measurements and to A. Boucheffa, B. Allegri (CNRS/LIMSI), D. Leroy and B. Szeless (CERN) for helpful discussions. B. Baudouy would like to thank Jeumont Schneider for financial support.

## References

[1] Burnod L, et al. Proceedings of 4th EPAC, 1994. p. 2295-7

[2] Baudouy B. Etude des transferts de chaleur dans les isolations électriques de cables supraconducteurs d'aimant d'accélérateur refroidi par hélium superfluide.Thèse de doctorat de l'Université Paris VI. Paris.1996.
[3] Baudouy B, et al. Steady-state heat transfer in He II through porous superconducting insulation. Adv. in Cryo. Eng. 1996;41 A:289.
[4] Baudouy B, et al. Thermal behavior of electrical multilayer insulation permeable to superfluid helium. Cryogenics 1996;ICEC Sup.:563.
[5] Conard G. Mesure de la conductibilité thermique du Kapton. CEA-Saclay, DSM/DAPNIA/STCM, Rapport de stage 1991.
[6] Staas FA, Taconis KW, and Van Alphen WM. Experiments on laminar and turbulent flow of He II in wide capillaries. Physica 1961;27:893.
[7] Landau LD and Lifshitz EM. Fluid Mechanics. 2 ed. Oxford: Butterworth-Heinemann, 1987.
[8] Vinen WF. Mutual friction in a heat current in liquid helium II - III. Theory of the mutual friction. *Proc. Roy. Soc.* 1957;A242:493-515.
[9] Ginzburg VL and Sobaynin AA. Superfluidity of helium II near the lambda point. Sov. Phy. Usp. 1974;19(10 October):773-812.
[10] Keller WE and Hammel EF. Isothermal flow of liquid He II through narrow channels. Physics 1966;2(5):221.
[11] Rudnick I, et al. Superfluid density in small pores. Physical Review Letters 1967;19(9):488-90.
[12] Ginzburg VL and Pitaevskii LP. On the theory of superfluidity. Sov. Phy. JETP 1958;7:858.

Table 1. Definition of electrical insulations

| | Insulation components | | | Equivalent thermal Characteristics | |
|---|---|---|---|---|---|
| | First layer Kapton 50 % overlap, 11-mm width | Second layer | Spacing | Resistance ($10^{-3}$ $Km^2W^{-1}$) | Conductivity ($10^{-3}$ $Wm^{-1}K^{-1}$) |
| B6 | 100 HN (25µ) | Prepreg fiberglass (120µ) | 2 mm | 9.5 ± 2.3 | 13.7 ± 3.8 |
| B15 | 100 HN | 2×120 XCI[a] (30µ) | 2 mm | 14.5 ± 2.7 | 10.4 ± 2.5 |
| B16 | 120 XCI[a] | 140 XRCI[a] (35µ) 50 % overlap | none | 19.7 ± 2.5 | 7.2 ± 1.0 |
| B18 | 100 HN | Prepreg fiberglass & dry fiberglass Kevlar tape (10.5 mm) | none | 9.8 ± 4.2 | 15.9 ± 6.2 |
| B21 | 100 HN | 2×140 XRCI[b] & dry fiberglass Kevlar tape | none | 13.7 ± 2.9 | 13.4 ± 3.3 |
| B21’ | 100 HN | 2×140 XRCI[b] | 10.5 mm | 12.9 ± 2.0 | 14.1 ± 2.5 |
| B22 | 150 HN (37.5µ) | 120 XCI[b] | 4 mm | 14.1 ± 2.6 | 10.1 ± 2.4 |
| B22’ | 150 HN | 120 XCI[b] | 2 mm | 14.9 ± 2.4 | 9.5 ± 1.7 |
| B25 | 50 HN (12.5µ) & 150 HN | 120 XCI[b] | 2 mm | 18.6 ± 3.4 | 9.3 ± 2.1 |

a: Adhesive Kapton (Polyimide glue on both sides) b: Adhesive Kapton (glue on the external layer side)

Table 2. Geometrical groups of the insulation sample B22

| $T_b$ | $(Ad^2/L)\ 10^{-14}\ m^3$ | $(A/L^{1/3})\ 10^{-5}\ m^{5/3}$ |
|---|---|---|
| 1.7 K | 53±5 | 3.14±0.10 |
| 1.8 K | 54±4 | 3.15±0.12 |
| 1.9 K | 48±4 | 3.11±0.07 |
| 2.0 K | 41±4 | 3.07±0.06 |
| 2.1 K | 26±5 | 3.50±0.24 |

Table 3. Geometrical groups of different insulations at 1.8 K.

| | $(Ad^2/L)$ $(10^{-14}\ m^3)$ | $(A/L^{1/3})$ $(10^{-5}\ m^{5/3})$ | $(A/L^{1/3})/A_t$ $(10^{-4}\ m^{-1/3})$ |
|---|---|---|---|
| B6 | - | 0.48 ± 0.03 | 4.8 |
| B15 | - | 0.96 ± 0.07 | 17.8 |
| B18 | - | 0.34 ± 0.01 | 3.4 |
| B21 | - | 2.82 ± 0.08 | 28.1 |
| B21’ | - | 5.98 ± 0.10 | 59.4 |
| B22 | 54.2 ± 4.2 | 3.15 ± 0.12 | 31.6 |
| B22’ | 9.2 ± 0.9 | 1.18 ± 0.04 | 11.8 |
| B25 | - | - | - |

Table 4. Equivalent cross section and thickness for samples B22 and B22'.

| | B22 | | B22' | |
|---|---|---|---|---|
| $T_b$ (K) | (A) ($10^{-6}$ $m^2$) | (d) (μm) | (A) ($10^{-6}$ $m^2$) | (d) (μm) |
| 1.7 | 6.98 | - | 2.55 | 21.2 |
| 1.8 | 7.00 | 29.0 | 2.62 | 19.8 |
| 1.9 | 7.01 | 27.8 | 2.61 | 17.8 |
| 2.0 | 6.82 | 25.7 | 2.64 | 16.2 |
| 2.05 | 7.04 | - | 2.81 | 15.5 |
| 2.1 | 7.79 | 19.1 | 3.1 | 13.2 |

**List of figures**

Figure 1. Schematic of insulation patterns

Figure 2. Schematic of the experimental apparatus

Figure 3. Different heat transfer regimes for the sample B22. The solid curves are the best fits to the data using equations (1) and (2) (including measurement errors).

Figure 4. Schematic of conduction and He II heat transfer paths.

Figure 5. Comparison between measurement and model for sample B15 at 1.902 K.

Figure 6. Comparison of different samples at 1.9 K. ¦ : B6, ∇ : B15, ? : B16, ¯ : B18, ◆ : B21, ? : B21', ? : B22, ? : B22' ,? : B25.

Figure 7. Temperature difference as a function of heat flux for sample B22' for different bath temperatures.

Figure 8. Evolution of $(Ad^2/L)$ as a function of bath temperature for sample B22 ? and B22' ? .

Figure 9. Evolution of $(Ad^2/L)$ as a function of $T'_{?}-T_b$ for sample B22'.

Cryogenics, Baudouy, Figure 1

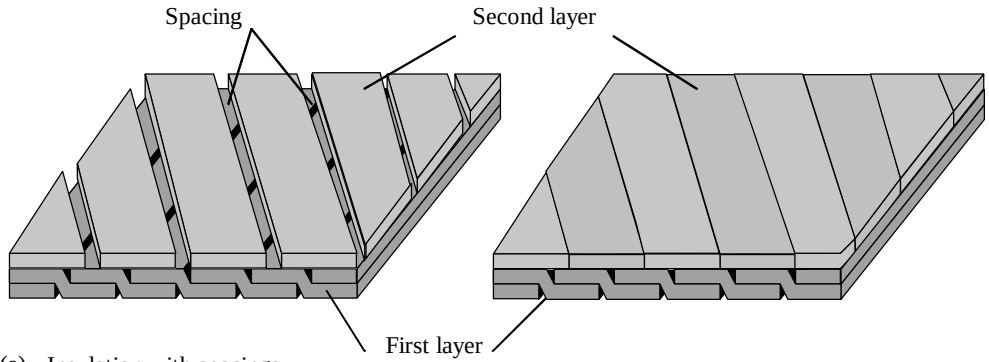


(a) Insulation with spacings

(b) Insulation without spacings

Cryogenics, Baudouy, Figure 2.

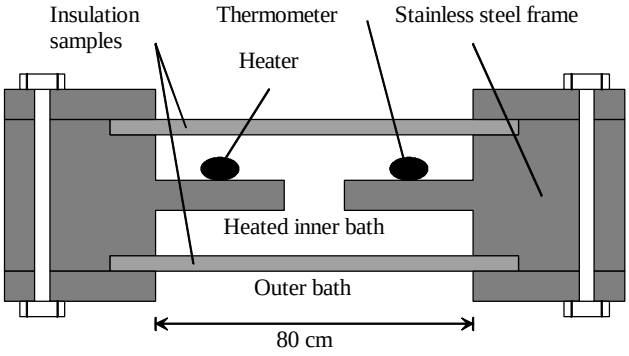

Cryogenics, Baudouy, Figure 3.

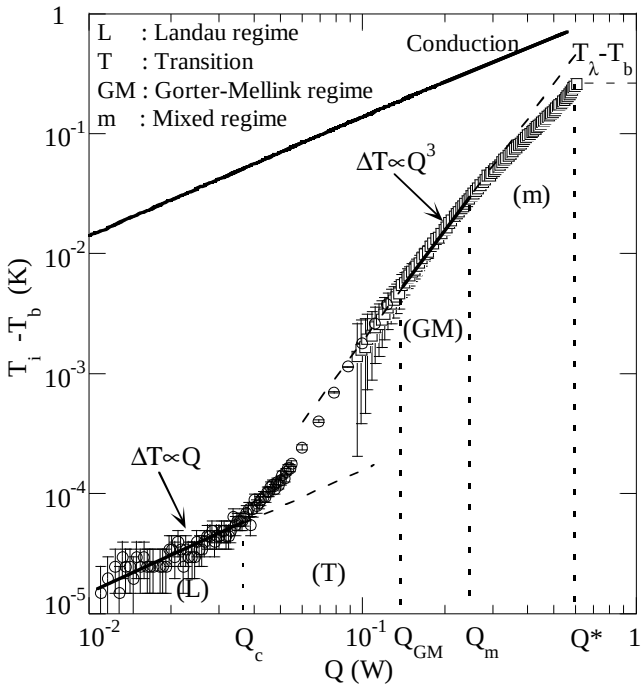

Cryogenics, Baudouy, Figure 4.

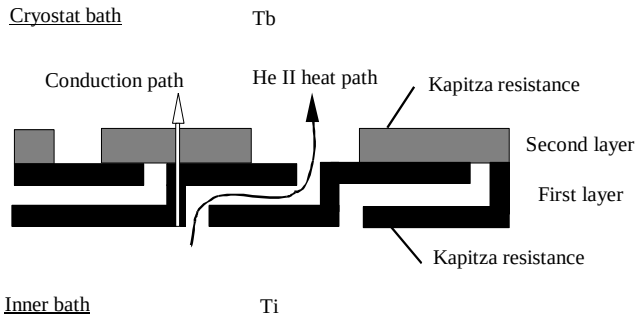

Cryogenics, Baudouy, Figure 5.

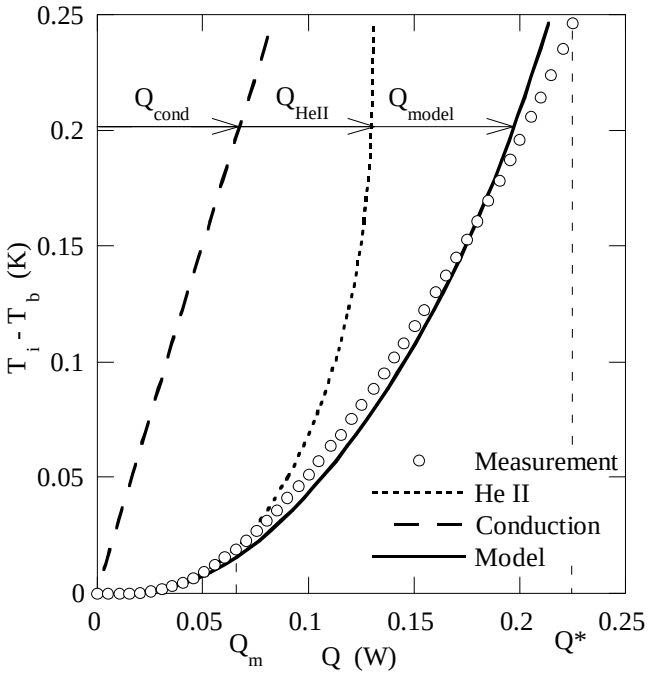

Cryogenics, Baudouy, Figure 6.

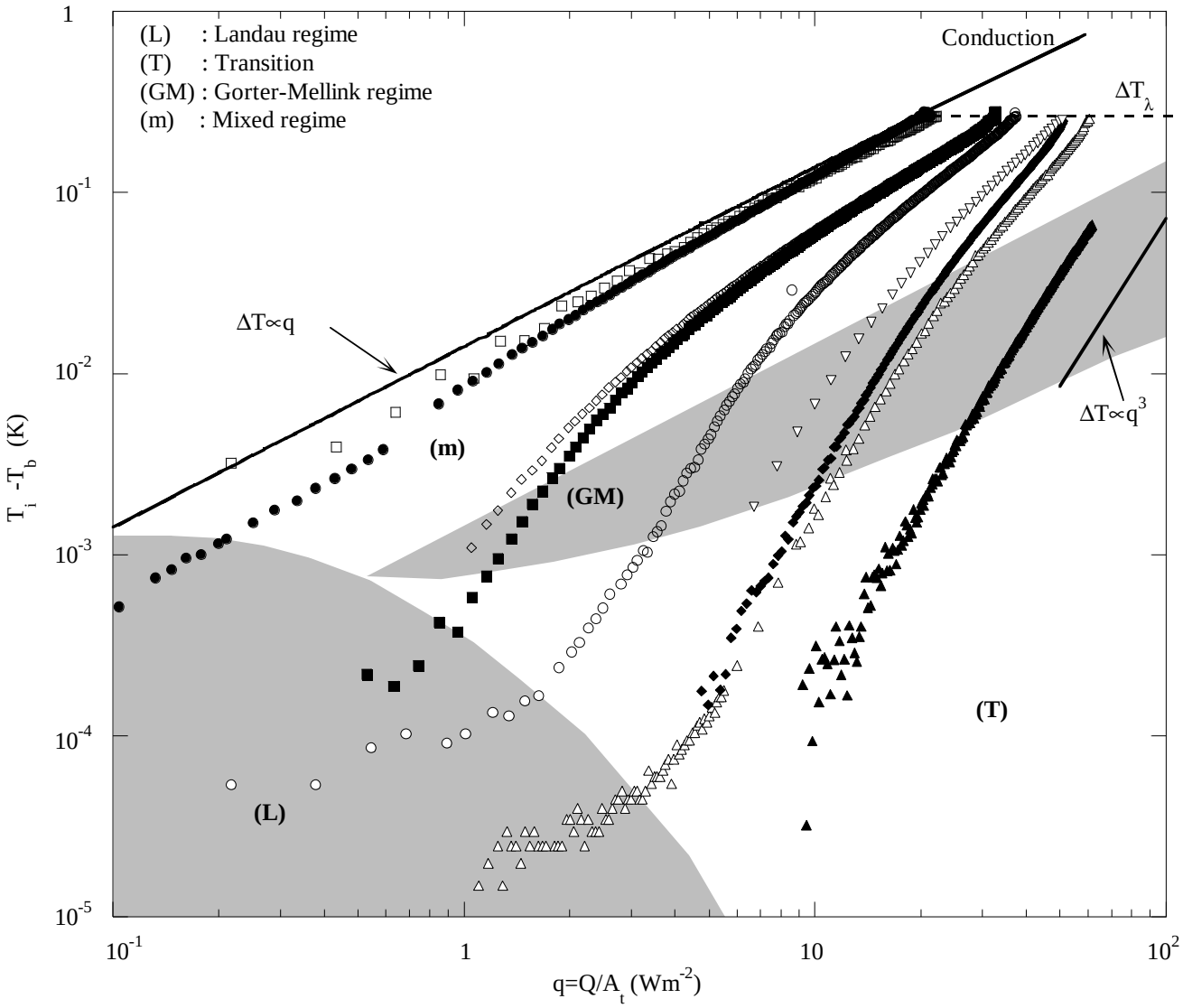

Cryogenics, Baudouy, Figure 7.

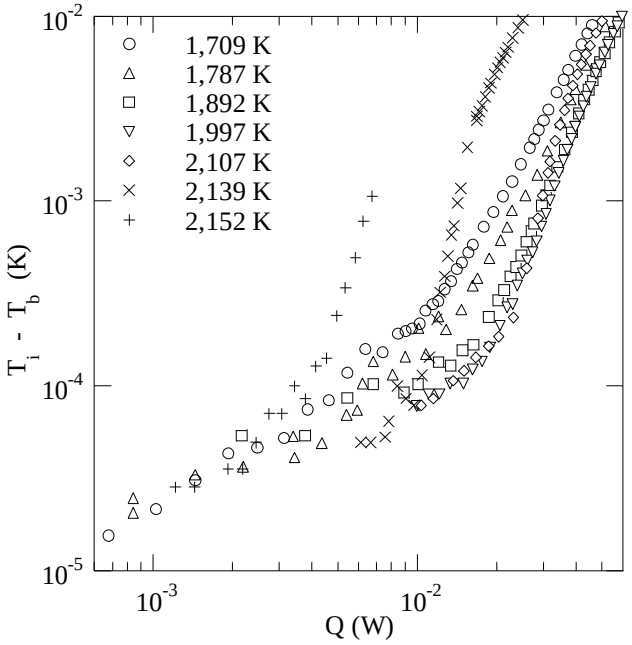

Cryogenics, Baudouy, Figure 8.

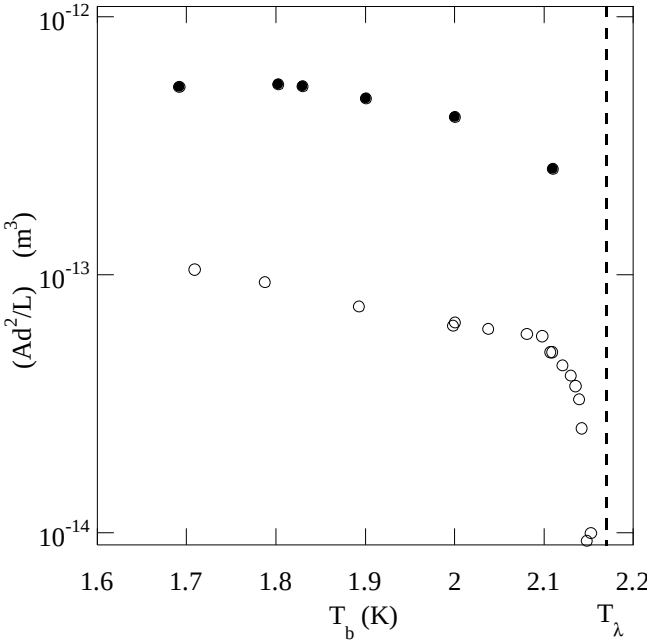

Cryogenics, Baudouy, Figure 9.